Mathematical Geology, Vol. 34, No. 3, April 2002 (© 2002)

Numerical Homogenization of the Rigidity Tensor in Hooke's Law Using the Node-Based Finite Element Method[1]

Wouter Zijl,[2] Max A. N. Hendriks,[3] and C. Marcel P. 't Hart[3]

Combining a geological model with a geomechanical model, it generally turns out that the geomechanical model is built from units that are at least a 100 times larger in volume than the units of the geological model. To counter this mismatch in scales, the geological data model's heterogeneous fine-scale Young's moduli and Poisson's ratios have to be "upscaled" to one "equivalent homogeneous" coarse-scale rigidity. This coarse-scale rigidity relates the volume-averaged displacement, strain, stress, and energy to each other, in such a way that the equilibrium equation, Hooke's law, and the energy equation preserve their fine-scale form on the coarse scale. Under the simplifying assumption of spatial periodicity of the heterogeneous fine-scale rigidity, homogenization theory can be applied. However, even then the spatial variability is generally so complex that exact solutions cannot be found. Therefore, numerical approximation methods have to be applied. Here the node-based finite element method for the displacement as primary variable has been used. Three numerical examples showing the upper bound character of this finite element method are presented.

KEY WORDS: periodic media, Poisson's ratio, upscaling, Young's modulus.

INTRODUCTION

The modeling of phenomena such as compaction of hydrocarbon reservoirs and aquifer–aquitard systems has traditionally been separated into geological and geomechanical modeling. These two activities reflect different aspects of the same part of the subsurface that is studied: the rock types that have developed during geological times, and their geomechanical behavior when placed under stress. The geological model highlights the structural elements of the subsurface—the geometry and dimensions of its layers and faults—together with its rock types

[1]Received 18 August 2000; accepted 29 March 2001.

[2]Netherlands Institute of Applied Geoscience TNO, P.O. Box 80015, NL-3508 TA Utrecht, The Netherlands; e-mail: w.zijl@nitg.tno.nl

[3]TNO Building and Construction Research, P.O. Box 49, NL-2600 AA Delft, The Netherlands; e-mail: m.hendriks@bouw.tno.nl; m.thart@bouw.tno.nl

and properties. The geomechanical model is set up in terms of quantities like displacement, strain, stress, and energy. These quantities are related to each other by the rock's rigidity parameters—Young's modulus and Poisson's ratio in isotropic rocks. When trying to match the geological and the geomechanical model, it generally turns out that the spatial scales of the two models differ. For example, the geological reservoir model may be based on cells meters in length and width and decimeters in thickness, whereas the geomechanical model is based on cells that are at least a 100 times larger in volume.

One approach to counter this mismatch in scales is to make the geomechanical model finer. This "megacell approach" will be made feasible by the next generation of multiprocessor computers (Dogru, 2000). However, there will always be a need to run geomechanical problems on relatively simple and cheap computers like PCs. In this way quick and user-friendly assessments can be made, even with run times that are sufficiently fast to be done in parallel with real-time measurements. In such a "fast model approach," the spatial scale of the cells in the geomechanical model must be chosen much coarser than in the megacell approach. Therefore, the heterogeneous fine-scale rock parameters of the geological data model have to be upscaled to "equivalent homogeneous" coarse-scale parameters that relate the cell-averaged displacement, strain, stress, and energy.

For upscaling of periodic media, homogenization theory is well established, both for the permeability in Darcy's law and for the rigidity in Hooke's law (Lefik and Schrefler, 1994; Pellegrino, Galvanetto, and Schrefler, 1999; Schrefler, Lefik, and Galvanetto, 1997). Classical homogenization theory is heavily based on the mathematics of functional analysis and multiscale asymptotic expansions (Auriault, 1983; Bakhvalov and Panasenko, 1994; Bensoussan, Lions, and Papanicolaou, 1978; Sanchez-Palencia, 1980). In this way, homogenization theory can deal with problems in which the course-scale equations have a form that differs from the fine-scale equations. However, here we consider a problem in which the fine-scale and coarse-scale equations have the same form. Therefore, it is possible to base homogenization on a simple principle that yields exactly the same results as classical homogenization. Based on the principle of "preservation of expressions," the coarse-scale rigidities are derived from the cell-averaged displacement, strain, stress, and energy, in such a way that well-known expressions on the fine scale are preserved, as much as possible, on the coarse scale. Following this idea, it will be shown that homogenization can be obtained by two independent procedures: displacement–stress averaging and displacement–energy averaging. If the medium is periodic, the two resulting coarse-scale rigidity tensors will be equal to each other (cf. Appendix for a proof). Because classical homogenization yields identical results, the term "homogenization" for our averaging approach is justified.

Since the resulting equations are generally too complex to be solved exactly, the node-based finite element method has been applied to solve the elliptic

equations for the displacement as primary variable. Displacement–energy averaging is then used to assess an error estimate of the finite element approximation. The theory is implemented in the finite element package DIANA (DIsplacement ANAlyzer), with which a number of numerical examples have been run.

THREE REQUIREMENTS FOR UPSCALING

Preferably, a procedure for upscaling of the rigidity should satisfy the following three requirements.

Requirement (i): Preservation of Expression for Strain

The coarse-scale displacement U_i should be equal to a spatial average $\langle u_i \rangle$ of the fine-scale displacement u_i while, *at the same time*, the coarse-scale displacement gradient $\partial_i U_j$ should be equal to the average displacement derivative $\langle \partial_i u_j \rangle$. If this requirement is satisfied, the coarse-scale strain, $E_{ij} = \langle \varepsilon_{ij} \rangle = \langle \partial_i u_j + \partial_j u_i \rangle / 2$, can be obtained as the symmetric part of the averaged displacement gradient, $E_{ij} = (\partial_i U_j + \partial_j U_i)/2$. This means that the fine-scale expression relating strain to displacement is preserved on the coarse scale.

The spatial averaging operator $\langle \cdot \rangle$ consistent with the above requirement is given by

$$\langle f \rangle(\underline{x}) = \frac{1}{\Delta x \Delta y \Delta z} \int_{x-\frac{1}{2}\Delta x}^{x+\frac{1}{2}\Delta x} \int_{y-\frac{1}{2}\Delta y}^{y+\frac{1}{2}\Delta y} \int_{z-\frac{1}{2}\Delta z}^{z+\frac{1}{2}\Delta z} f(\underline{x}')\, dx'\, dy'\, dz' \qquad (1)$$

($\underline{x}$ denotes the row of Cartesian coordinates (x, y, z)). In this paper, the upscaling cell is a rectangular hexahedron (a block). Then $x_i = \langle x_i \rangle$ denotes a Cartesian coordinate and Equation (1) represents volume averaging. However, if the cell has another shape, for instance a cylindrical cell around a well, x_i represents a curvilinear orthogonal coordinate, for which averaging is not *volume*-averaging (Zijl and Trykozko, 2001).

Requirement (ii): Preservation of Expression for Stress Divergence

The second requirement is that the coarse-scale stress Σ_{ij} should be equal to the averaged fine-scale stress $\langle \sigma_{ij} \rangle$. If requirement (ii) is satisfied, it follows from Equation (1) that $\langle \partial_i \sigma_{ij} \rangle = \partial_i \langle \sigma_{ij} \rangle = \partial_i \Sigma_{ij}$. This way the divergence of the stress, which plays a dominant role in the equilibrium equation, has the same from on the coarse scale as on the fine scale.

Requirement (iii): Preservation of Expression for Energy

The third requirement is that the coarse-scale energy $\Phi = E_{ij}\Sigma_{ij}$ should be equal to the average of the fine-scale energy $\langle\phi\rangle = \langle\varepsilon_{ij}\sigma_{ij}\rangle$. This requirement expresses that the energy equation for the fine scale is preserved on the coarse scale. The energy defined above equals *two times* the amount of reversible elastic energy stored in the upscaling cell, divided by the volume of the cell. If requirement (iii) is satisfied, thermodynamic expressions—like energy potentials, Onsager's reciprocal relations, etc.—have the same form on the coarse scale as on the fine scale.

Unfortunately, for general heterogeneous media the above three requirements overspecify the upscaling problem. However, both perfectly layered porous media and *periodic* porous media can be upscaled in such a way that the three requirements are satisfied simultaneously. Then the above upscaling approach leads to the same results as classical homogenization.

THREE UPSCALING APPROACHES PRESERVING HOOKE'S LAW

Classical homogenization theory can deal with problems in which the course-scale expressions differ from the fine-scale expression. However, because we do not consider such a problem, we may require that Hooke's law on the fine scale be preserved on the coarse scale. In the previous section we have already introduced the principle of "preservation of expressions." This section presents an extension to the three possible ways in which Hooke's fine-scale law can be preserved on the coarse scale. Since, in general, only two of the three requirements of the previous section can be satisfied simultaneously, upscaling based on volume averaging can be performed in the following three ways.

Displacement–Stress (DS) Averaging

Displacement–stress (DS) averaging combines requirements (i) and (ii) using $\langle\sigma_{\alpha\beta ij}\rangle = C^{(\mathrm{DS})}_{ijmn}\langle\varepsilon_{\alpha\beta mn}\rangle$ to define the coarse-scale rigidity $C^{(\mathrm{DS})}_{ijmn}$. The first two indices, $\alpha, \beta = 1, 2, 3$, denote the nine different load cases that have to be solved in order to find all the 81 components of the coarse-scale rigidity tensor. The second two indices, $i, j = 1, 2, 3$, denote Cartesian components. The inverse of the rigidity, the compliance tensor, will be denoted as $S^{(\mathrm{DS})}_{ijmn}$. If $\langle\varepsilon_{mnij}\rangle$ is chosen equal to $(\delta_{in}\delta_{jm} + \delta_{im}\delta_{jn})/2$ (δ_{ij} is the Kronecker delta function), we find $C^{(\mathrm{DS})}_{ijmn} = \langle\sigma_{mnij}\rangle$.

Displacement–Energy (DE) Averaging

Displacement–energy (DE) averaging combines requirements (i) and (iii) using $\langle\varepsilon_{\alpha\beta ij}\rangle C^{(\mathrm{DE})}_{ijmn}\langle\varepsilon_{\gamma\delta mn}\rangle = \langle\phi_{\alpha\beta\gamma\delta}\rangle$ to define the coarse-scale rigidity $C^{(\mathrm{DE})}_{ijmn}$. Here

$\phi_{\alpha\beta\gamma\delta} = \varepsilon_{\alpha\beta ij}\sigma_{\gamma\delta ij}$ is a component of the fine-scale energy matrix. If $\langle\varepsilon_{mnij}\rangle$ is chosen equal to $(\delta_{in}\delta_{jm} + \delta_{im}\delta_{jn})/2$, we find $C^{(\mathrm{DE})}_{ijmn} = \langle\phi_{ijmn}\rangle$. The compliance tensor will be denoted as $C^{(\mathrm{DE})}_{ijmn}$.

Stress–Energy (SE) Averaging

Stress–energy (SE) averaging combines requirements (ii) and (iii) using $\langle\sigma_{\gamma\delta ij}\rangle S^{(\mathrm{SE})}_{ijmn}\langle\sigma_{\alpha\beta mn}\rangle = \langle\phi_{ijmn}\rangle$ to define the coarse-scale compliance tensor $S^{(\mathrm{SE})}_{ijmn}$, which is the inverse of the coarse-scale rigidity $C^{(\mathrm{SE})}_{ijmn}$. Since $S^{(\mathrm{SE})}_{ijmn} = S^{(\mathrm{DS})}_{\alpha\beta ij}C^{(\mathrm{DE})}_{\alpha\beta\gamma\delta}S^{(\mathrm{DS})}_{\gamma\delta mn}$, only displacement–stress and displacement–energy averaging will be discussed ahead.

Choice of Homogenization Cells

Because the fine-scale rigidity tensor c_{ijmn} is symmetric ($c_{ijmn} = c_{mnij}$) and strictly positive definite, it follows from the above definitions that also the coarse-scale rigidity tensors $C^{(\mathrm{DE})}_{ijmn}$ and $C^{(\mathrm{SE})}_{ijmn}$ are symmetric and strictly positive definite. The coarse-scale rigidity tensor $C^{(\mathrm{DS})}_{ijmn}$ will generally be nonsymmetric (Rijpsma and Zijl, 1998).

Both for layered and *periodic* media the three upscaling approaches yield the same coarse-scale rigidity, that is, $C^{(\mathrm{DS})}_{ijmn} = C^{(\mathrm{DE})}_{ijmn} = C^{(\mathrm{SE})}_{ijmn} = C_{ijmn}$ (for periodic media this is proved in the Appendix). Of course, natural media are neither layered nor periodic, but in many practical cases one can distinguish subdomains in which layering or periodicity may be considered as an approximation.

HOMOGENIZATION BASED ON A PHYSICAL POINT OF VIEW

In periodic media the fine-scale rigidity has translation symmetry in three different directions. For such media the smallest possible homogenization cell is a parallelepiped with edges that represent the periodicity interval of the translation symmetry.

The Basic Equation

Homogenization is an upscaling method for periodic media. Classical homogenization is based on a mathematical point of a view, in which functional analysis and multiscale asymptotic expansions play the dominant role (Bensoussan, Lions, and Papanicolaou, 1978; Hornung, 1997; Sanchez-Palencia, 1980). Here, a much simpler approach to homogenization is introduced. This approach is

based on a physical point of view and yields exactly the same results as classical homogenization.

The basis of our "physical approach" is to *equate* the net fine-scale force working on a domain with closed boundary, $\oiint n_i \sigma_{ij}\, dS + \iiint f_j\, dV$, to the net coarse-scale force working on the same domain, $\oiint n_i \Sigma_{ij}\, dS + \iiint F_j\, dV$, where f_i and F_i are respectively the fine-scale and coarse-scale body force. Since $\iiint f_i\, dV = \langle f_i \rangle V$, defining $F_i = \langle f_i \rangle$ yields $\iiint f_i\, dV = \iiint F_i\, dV$. Hence the basis of our approach simplifies to $\oiint n_i \sigma_{ij}\, dS = \oiint n_i \Sigma_{ij}\, dS$. Using Gauss's integral theorem and substituting Hooke's law yields

$$\partial_i(c_{ijmn}(\partial_m u_n + \partial_n u_m)) = \partial_i(C_{ijmn}(\partial_m U_n + \partial_n U_m)) \tag{2}$$

Equation (2) will be used in two different ways: (i) to determine the fine-scale equations that have to be solved numerically, and (ii) to prove the equivalence between DS and DE averaging: cf. Appendix.

The Fine-Scale Equation and Boundary Conditions

Equation (2) can be simplified by invoking a "smoothness requirements." Let us consider a coarse-scale map with scale ϑ and "map coordinates" $y_i = \vartheta x_i$. For instance, if the map has scale $\vartheta = 1{:}100000$, a distance $y_i = 1$ cm on the map corresponds to a distance $x_i = 1$ km in reality. On the coarse-scale map the fine-scale details are smoothed away: a variation of the coarse-scale stress $\Sigma_{ij}(\underline{y})$ over a map distance $\Delta y = \ell$ (i.e., over the much larger real distance $\Delta x = \ell/\vartheta$) has at most the same order of magnitude as a variation of the fine-scale stress $\sigma_{ij}(\underline{x})$ over a real distance $\Delta x = \ell$. Equation (2) yields $\partial \sigma_{ij}(\underline{x})/\partial x_i = \vartheta\, \partial \Sigma_{ij}(\underline{y})/\partial y_i$ and substitution of the perturbation series $\sigma_{ij} = \sigma_{ij}^{(0)} + \vartheta \sigma_{ij}^{(1)} \ldots$ while equating terms of the same power of ϑ (Van Dyke, 1975) produces the fine-scale equation of order zero $\partial_i \sigma_{ij}^{(0)}(\underline{x}) = 0$. Omitting the superscript (0) and substituting Hooke's law, Equation (2) is approximated by the following fine-scale equation

$$\partial_i(c_{ijmn}(\partial_m u_n + \partial_n u_m)) = 0 \tag{3}$$

For periodic media, where Σ_{ij} is constant with respect to the fine scale, $\vartheta = 0$, that is, Equation (3) is exact. Then the coarse-scale rigidity C_{ijmn} is constant too and, according to Hooke's coarse-scale law $\Sigma_{ij} = C_{ijmn} E_{mn}$, also the coarse-scale strain E_{ij} is constant. Moreover, since $E_{ij} = (\partial_i U_j + \partial_i U_j)/2$, the coarse-scale displacement is linear in x_i, that is, $U_i(\underline{x}) = U_i^{(0)} + A_{ij} x_j$ with $E_{ij} = (A_{ij} + A_{ji})/2$ (Appendix). Both for displacement–stress (DS) averaging and for

displacement–energy (DE) averaging we have already required that $U_i = \langle u_i \rangle$ and $E_{ij} = \langle \varepsilon_{ij} \rangle$. Then the fine-scale displacement is equal to the coarse-scale displacement plus a periodic "correction" χ_i that has the same periodicity pattern as the fine-scale rigidity c_{ijmn} (for a proof cf. Appendix).

Equation (3) has to be solved, either analytically or numerically, in at least one periodicity cell. The boundary conditions have to be such that the function $\chi_i(\underline{x}) = u_i(\underline{x}) - A_{ij}x_j$ is periodic. In other words, the boundary conditions for the displacement are such that the displacement differences between two similar points on opposite boundaries are constant (Appendix). In this way, nine linear independent sets of boundary conditions or "load cases," denoted by $\alpha, \beta = 1, 2, 3$ can be defined (Fig. 1).

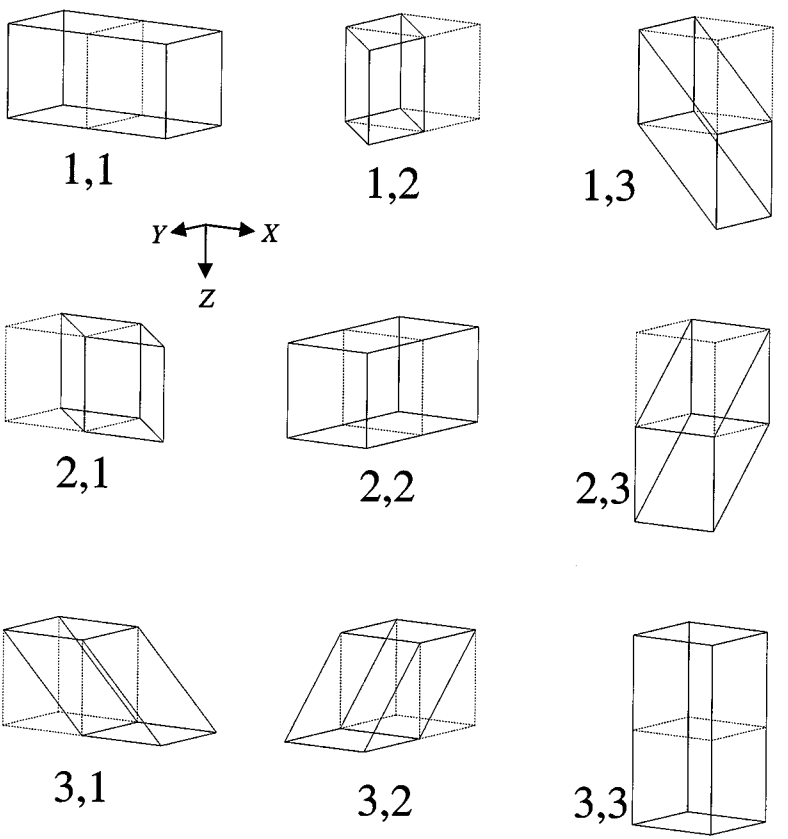

Figure 1. Deformations of homogeneous isotropic cell with $\nu = 0$ for nine orthonormal load cases $\alpha, \beta = 1, 2, 3$.

Determination of the Coarse-Scale Laws and Parameters

Scalar multiplication of Equation (2) for $u_i = u_{\alpha\beta i}$ and $U_i = U_{\alpha\beta i}$ by a different fine-scale displacement $u_{\gamma\delta i}$, applying Gauss's divergence theorem, and using the periodicity, yields

$$\Sigma_{\alpha\beta ij} = \langle \sigma_{\alpha\beta ij} \rangle \Leftrightarrow \langle \varepsilon_{\alpha\beta ij} \rangle C_{ijmn} \langle \varepsilon_{\gamma\delta mn} \rangle = \langle \varepsilon_{\alpha\beta ij} \sigma_{\gamma\delta ij} \rangle \tag{4}$$

Appendix, from which it follows that the DS, DE, and SE averaging approaches yield equivalent results.

In conclusion, the coarse-scale Hooke's law is $\Sigma_{ij} = C_{ijmn}(\partial_m U_n + \partial_n U_m)/2$ in which C_{ijmn} is the coarse-scale rigidity tensor and the coarse-scale energy equation is $\Phi_{ijmn} = E_{ijkl}\Sigma_{mnkl}$. The coarse-scale equilibrium equation can be obtained by averaging the fine-scale equilibrium equation $\partial_i \sigma_{ij} = -f_j$ yielding $\partial_i \langle \sigma_{ij} \rangle = -\langle f_j \rangle$.

Orthonormal Boundary Conditions

In general, homogenization theory requires that the displacements on two opposite boundaries of the rectangular homogenization cell have a constant difference $\Delta_j u_{mni} = k_{ijmn}$, where $\Delta_j u_{mni} = u_{mni}(x_j + \frac{1}{2}\Delta x_j) - u_{mni}(x_j - \frac{1}{2}\Delta x_j)$ denotes the difference in direction j of displacement component i between two equivalent points on opposite boundaries of the homogenization cell. The indices $m, n = 1, 2, 3$ denote nine different displacement vectors, each with three components u_{mni}, $i = 1, 2, 3$.

The choice of orthonormal boundary conditions

$$\Delta_j u_{mni} = \delta_{in}\delta_{jm}\Delta x_j \quad \text{(no summation over index } j\text{)} \tag{5}$$

is very convenient. For example, if $m = 2$ and $n = 1$, boundary condition (5) denotes a constant displacement difference $\Delta_y u_{21x} = \Delta y$ between the two opposite boundaries in the y direction, and zero displacement differences $\Delta_z u_{21x} = \Delta_x u_{21x} = 0$ between the two opposite boundaries in the z and x directions. In addition, also the differences of displacement components u_{21y} and u_{21z} between all opposite boundaries are equal to 0.

Using orthonormal boundary conditions (5), the coarse-scale displacement is $U_{mni} = \langle u_{mni} \rangle = \delta_{in} x_m$, from which it follows that the coarse-scale strain is $E_{mnij} = \langle \varepsilon_{mnij} \rangle = (\delta_{in}\delta_{jm} + \delta_{im}\delta_{jn})/2$. Substitution into Hooke's law and using Equation (4) yields very simple expressions for the homogenized rigidity:

displacement–stress (DS) averaging yields $C_{ijmn} = \langle \sigma_{mnij} \rangle$, and displacement–energy (DE) averaging yields $C_{ijmn} = \langle \phi_{ijmn} \rangle$.

NUMERICAL HOMOGENIZATION USING FINITE ELEMENTS

Node-Based Finite Elements for the Displacement

Homogenization software has been implemented in the node-based finite element package DIANA (DIsplacement ANAlyzer) with nodal displacements as degrees of freedom. The mesh has been chosen uniform with equally sized eight-noded "solids" (blocks). The approximation space consists of piecewise bilinear functions. DIANA's "tyings" option has been used to model boundary conditions with constant displacement difference (De Witte and Hendriks, 1998). In general, a tying is a user specified linear dependency between degrees of freedom of the system of equations. In case of homogenization, tyings between two opposite boundary points enforce the same displacement plus a constant. This way the nine orthonormal load cases $\alpha, \beta = 1, 2, 3$ have been implemented and applied (Fig. 1).

For all nine load cases DIANA computes in each solid block the six strain components $\varepsilon_{\alpha\beta xx}, \varepsilon_{\alpha\beta yy}, \varepsilon_{\alpha\beta zz}, \gamma_{\alpha\beta xy} = \gamma_{\alpha\beta yx}, \gamma_{\alpha\beta yz} = \gamma_{\alpha\beta zy}, \gamma_{\alpha\beta zx} = \gamma_{\alpha\beta xz}$ ($\gamma_{\alpha\beta,ij} = 2\varepsilon_{\alpha\beta,ij}$ are the "technical strains") yielding 54 volume averaged strain components $E_{\alpha\beta ij}$. Moreover, the orthogonal load cases lead to 18 additional symmetry conditions $E_{\alpha\beta ij} = E_{\beta\alpha ij}$. This means that only six load cases are linear independent, yielding 36 independent coarse-scale strain components and, according to Hooke's law, 36 coarse-scale stress components. For all six relevant load cases $\gamma, \delta = 1, 2, 3$ DIANA computes in each solid block the six stress components $\sigma_{\gamma\delta xx}, \sigma_{\gamma\delta yy}, \sigma_{\gamma\delta zz}, \sigma_{\gamma\delta xy} = \sigma_{\gamma\delta yx}, \sigma_{\gamma\delta yz} = \sigma_{\gamma\delta zy}, \sigma_{\gamma\delta zx} = \sigma_{\gamma\delta xz}$. These stresses are volume averaged by approximating the volume integrals over each solid block by a $2 \times 2 \times 2$ Gaussian integration scheme. This yields 36 volume averaged stress components $\Sigma_{\gamma\delta ij}$. Moreover, using $\phi_{\alpha\beta\gamma\delta} = \varepsilon_{\alpha\beta xx}\sigma_{\gamma\delta xx} + \varepsilon_{\alpha\beta yy}\sigma_{\gamma\delta yy} + \varepsilon_{\alpha\beta zz}\sigma_{\gamma\delta zz} + \gamma_{\alpha\beta xy}\sigma_{\gamma\delta xy} + \gamma_{\alpha\beta yz}\sigma_{\gamma\delta yz} + \gamma_{\alpha\beta zx}\sigma_{\gamma\delta zx}$ yields 36 volume averaged energies $\Phi_{\alpha\beta\gamma\delta}$. Displacement–stress (DS) averaging yields the coarse-scale rigidity tensor $C^{(\mathrm{DS})}_{ijmn} = \Sigma_{mnij}$ and displacement–energy (DE) averaging yields the coarse-scale rigidity tensor $C^{(\mathrm{DE})}_{ijmn} = \Phi_{ijmn}$.

Error Bounds for Numerical Homogenization

For symmetric and strictly positive definite fine-scale rigidity tensors c_{ijmn}, the "principle of least action" holds (Duvaut and Lions, 1976; Lanczos, 1970; Morse and Feshbach, 1953). This principle states that the solution $u_{\alpha\beta i}$ of Equation (3) is the function $\theta_{\alpha\beta i}$ that minimizes the strictly positive definite functional

$4\Theta(\underline{\theta}_{\alpha\beta}) = \langle(\partial_i\theta_{\alpha\beta j} + \partial_j\theta_{\alpha\beta i})c_{ijmn}(\partial_m\theta_{\alpha\beta n} + \partial_n\theta_{\alpha\beta m})\rangle > 0$ for all functions $\theta_{\alpha\beta i}(\underline{x})$ with $\theta_{\alpha\beta i}(\underline{x}_B) = u_{\alpha\beta i}(\underline{x}_B)$ on the closed boundary $\underline{x} \in \partial\Omega$ of domain Ω ($\underline{\theta}_{\alpha\beta}$ is the row of components $\theta_{\alpha\beta x}, \theta_{\alpha\beta y}, \theta_{\alpha\beta z}$).

Displacement–energy averaging defines the coarse-scale rigidity tensor C_{ijmn} by $(\partial_i U_{\alpha\beta j} + \partial_j U_{\alpha\beta i})C_{ijmn}(\partial_m U_{\gamma\delta n} + \partial_n U_{\gamma\delta m}) = \langle(\partial_i u_{\alpha\beta j} + \partial_j u_{\alpha\beta i})c_{ijmn}(\partial_m u_{\gamma\delta n} + \partial_n u_{\gamma\delta m})\rangle$. Orthonormal boundary condition (5) yields $\partial U_{\alpha\beta i}/\partial x_j = \delta_{i\beta}\delta_{j\alpha}$ and, hence, $4C_{\alpha\beta\gamma\delta} = \langle(\partial_i u_{\alpha\beta j} + \partial_j u_{\alpha\beta i})c_{ijmn}(\partial_m u_{\gamma\delta n} + \partial_n u_{\gamma\delta m})\rangle$. This means that $C_{ijij} = \Theta(\underline{u}_{ij}) > 0$ and, as a consequence of the variational principle, displacement fields $\underline{u}_{ij}$ are such that the diagonal components C_{ijij} are minimal.

To find approximate, solutions, Equation (3) is solved by the node-based finite element method for the displacement. This method is equivalent with the Ritz method (Strang and Fix, 1973), which is based on the principle of least action to find nodal displacements that minimize the energy in the domain. Therefore, this approximation method minimizes the functional $\Theta(\underline{\theta}_{\alpha\beta}) > 0$. However, in general the approximation space differs from the function space of the exact solution, which means that the exact minimum cannot be obtained and, as a result, the approximate energy is greater than the exact energy. In other words, the rock is approximated as too rigid. Of course, when the exact solution is in the approximation space, the finite element solution is equal to the exact solution. As a consequence, denoting the node-based approximation of the rigidity by C^{NB}_{ijmn}, we find $E_{\alpha\beta ij}C^{\mathrm{NB}}_{ijmn}E_{\alpha\beta mn} \geq E_{\alpha\beta ij}C_{ijmn}E_{\alpha\beta mn} > 0$, from which it follows that $C^{\mathrm{NB}}_{ijij} \geq C_{ijij}$ in any arbitrary coordinate system. Because the approximate solution comes closer to the exact solution when the grid is refined, the diagonal elements will monotonously approach the exact asymptote.

There exist "complementary" numerical methods for which the same inequality holds for the compliance tensor S_{ijmn}, which is the inverse of the rigidity tensor C_{ijmn}. Face-based (mixed hybrid) finite element methods for the facial tractions (Bossavit, 1998; Penman, 1988; Trykozko, Zijl, and Bossavit, 2000) and block-centered finite difference methods (Arbogast, Wheeler, and Yotov, 1997) are such complementary methods. These methods yield coarse-scale rigidities that represent the mechanical properties as too weak. It is customary define the coarse-scale rigidity matrix as the 6×6 matrix that relates the six coarse-scale stress components (Σ_{xx}, Σ_{yy}, Σ_{zz}, Σ_{xy}, Σ_{yz}, Σ_{zx}) to the six coarse-scale strain components (E_{xx}, E_{yy}, E_{zz}, Γ_{xy}, Γ_{yz}, Γ_{zx}); here $\Gamma_{ij} = 2E_{ij}$ are the "technical strains." The inverse of this matrix is the coarse-scale compliance matrix. It can be proved that the eigenvalues of the coarse-scale *rigidity* matrix calculated using the *node-based* method are upper bounds. In addition, the eigenvalues of the coarse-scale *compliance* matrix calculated using *complementary* methods are upper bounds too (Bossavit, 1998; Trykozko, Zijl, and Bossavit, 2000). Since the eigenvalues of the compliance matrix are the inverses of the eigenvalues of the rigidity matrix, node-based and complementary methods can be used together to confine the numerical approximation error in an interval between upper and a lower bounds.

NUMERICAL EXAMPLES

Perfectly Layered Rock

This example considers a perfectly layered linear elastic rock that is isotropic on the fine scale. Since strain and stress depend only on the z coordinate, Hooke's law $\sigma_{ij} = \lambda\varepsilon_{kk}\delta_{ij} + 2\mu\varepsilon_{ij}$ substituted into equilibrium Equation (3) simplifies to $\partial_z(\mu(\partial_z u_x + \partial_x u_z)) = 0$, $\partial_z(\mu(\partial_z u_y + \partial_y u_z)) = 0$, $\partial_z(\eta\partial_z u_z + \lambda(\partial_x u_x + \partial_y u_y)) = 0$. Here $\eta = e(1-\nu)(1+\nu)^{-1}(1-2\nu)^{-1}$, $\lambda = e\nu(1+\nu)^{-1}(1-2\nu)^{-1}$, $\mu = e(1+\nu)^{-1}/2$, where $e = e(z)$ and $\nu = \nu(z)$ are respectively the fine-scale Young's modulus and Poisson's ratio.

The nine fine-scale displacement vectors that satisfy the equilibrium equations and the orthonormal boundary conditions are

$$(u_{11x}, u_{11y}, u_{11z}) = \left(x, 0, \int \eta(z)^{-1}\{\langle\lambda\eta^{-1}\rangle\langle\eta^{-1}\rangle^{-1} - \lambda(z)\}\, dz\right) \tag{6.1}$$

$$(u_{22x}, u_{22y}, u_{22z}) = \left(0, y, \int \eta(z)^{-1}\{\langle\lambda\eta^{-1}\rangle\langle\eta^{-1}\rangle^{-1} - \lambda(z)\}\, dz\right) \tag{6.2}$$

$$(u_{33x}, u_{33y}, u_{33z}) = \left(0, 0, \langle\eta^{-1}\rangle^{-1}\int \eta(z)^{-1}\, dz\right) \tag{6.3}$$

$$(u_{12x}, u_{12y}, u_{12z}) = (0, x, 0) \tag{6.4}$$

$$(u_{21x}, u_{21y}, u_{21z}) = (y, 0, 0) \tag{6.5}$$

$$(u_{23x}, u_{23y}, u_{23z}) = \left(0, \langle\mu^{-1}\rangle^{-1}\int \mu(z)^{-1}\, dz - z, y\right) \tag{6.6}$$

$$(u_{32x}, u_{32y}, u_{32z}) = \left(0, \langle\mu^{-1}\rangle^{-1}\int \mu(z)^{-1}\, dz, 0\right) \tag{6.7}$$

$$(u_{31x}, u_{31y}, u_{31z}) = \left(\langle\mu^{-1}\rangle^{-1}\int \mu(z)^{-1}\, dz, 0, 0\right) \tag{6.8}$$

$$(u_{13x}, u_{13y}, u_{13z}) = \left(\langle\mu^{-1}\rangle^{-1}\int \mu(z)^{-1}\, dz - z, 0, x\right) \tag{6.9}$$

In this example, the parameters η, λ, and μ are chosen piecewise constant, yielding a piecewise linear solution. Because in this example the piecewise bilinear approximation space of the finite elements contains the space of the exact solution, the finite element solution is equal to the exact solution. Therefore, the small differences between numerical and exact solution are caused by inaccuracies in the solution of the algebraic equations.

From solutions (6) the fine-scale strains and, using Hooke's law, the fine-scale stresses can be calculated, as well as the fine-scale elastic energies $\phi_{ijmn} = \varepsilon_{ijkl}\sigma_{mnkl}$. It turns out that only 25 fine-scale energy and 21 fine-scale stress components are nonzero. Volume averaging of the fine-scale energy and stress components yields 21 nonzero coarse-scale energy components $\Phi_{ijmn} = \langle\phi_{ijmn}\rangle$ and stress components $\Sigma_{mnij} = \langle\sigma_{mnij}\rangle$. Moreover, we find $\Sigma_{mnij} = \Phi_{ijmn} = C_{ijmn}$. As a consequence, the coarse-scale Hooke's law is

$$\begin{pmatrix} \Sigma_{xx} \\ \Sigma_{yy} \\ \Sigma_{zz} \\ \Sigma_{xy} \\ \Sigma_{yz} \\ \Sigma_{zx} \end{pmatrix} = \begin{pmatrix} T^2R + 4(M-S) & T^2R + 2M - 4S & TR & 0 & 0 & 0 \\ T^2R + 2M - 4S & T^2R + 4(M-S) & TR & 0 & 0 & 0 \\ TR & TR & R & 0 & 0 & 0 \\ 0 & 0 & 0 & M & 0 & 0 \\ 0 & 0 & 0 & 0 & L & 0 \\ 0 & 0 & 0 & 0 & 0 & L \end{pmatrix} \cdot \begin{pmatrix} E_{xx} \\ E_{yy} \\ E_{zz} \\ \Gamma_{xy} \\ \Gamma_{yz} \\ \Gamma_{zx} \end{pmatrix} \quad (7)$$

where $L = \langle\mu^{-1}\rangle^{-1},\ M = \langle\mu\rangle,\ R = \langle\eta^{-1}\rangle^{-1},\ S = \langle\mu^2\eta^{-1}\rangle,\ T = 1 - 2\langle\mu\eta^{-1}\rangle$ are the "Backus parameters."

Figure 2 shows the mesh consisting of $10 \times 10 \times 10$ elements. Figure 3 and Table 1 present the piecewise constant fine-scale rigidities. Table 2 shows the

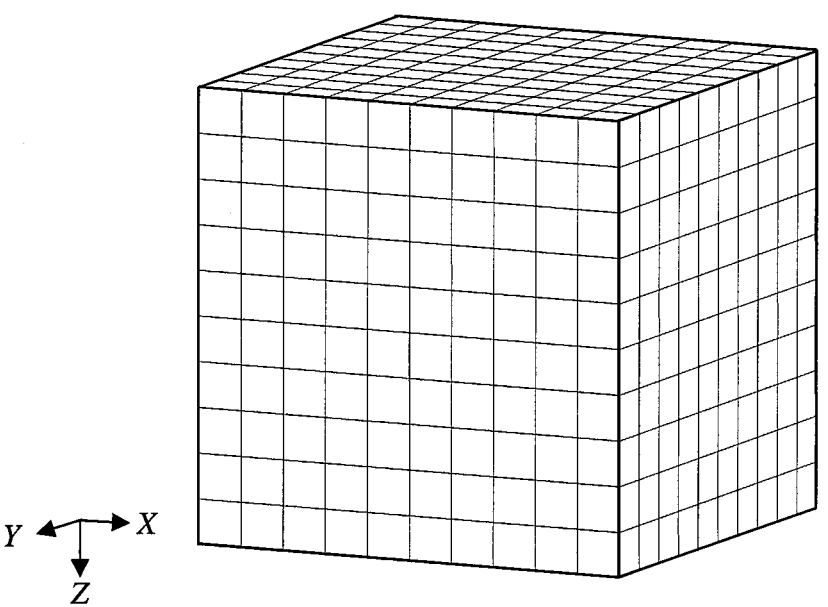

Figure 2. Finite element mesh in the homogenization cell.

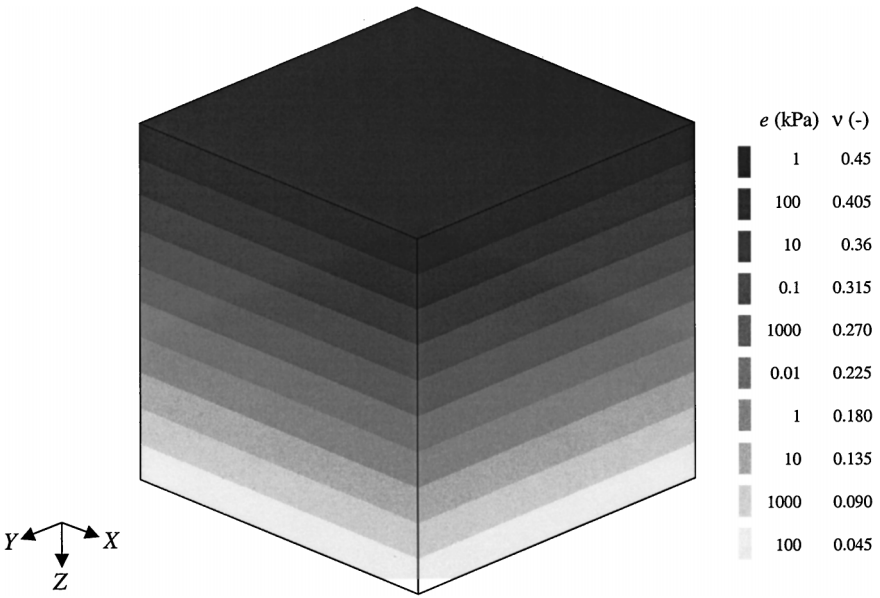

Figure 3. Homogenization cell filled with perfectly layered fine-scale parameters.

Backus parameters leading to the exact rigidity components presented in Table 3. The numerical approximations are presented in Tables 4 and 5 for respectively displacement–stress and displacement–energy averaging. The numerical approximations of the coarse-scale rigidities differ by less than 1‰ from the exact values.

Table 1. Perfectly Layered Rock With Piecewise Constant Fine-Scale Young's Moduli and Poisson's Ratios

Layer	e (kPa)	ν (−)
1	1	0.450
2	100	0.405
3	10	0.360
4	0.1	0.315
5	1000	0.270
6	0.01	0.225
7	1	0.180
8	10	0.135
9	1000	0.090
10	100	0.045

Table 2. Backus Parameters

L (kPa)	0.035351296
M (kPa)	85.33762335
R (kPa)	0.109754705
S (kPa)	22.84657428
T (−)	0.370299677

Continuous Fine-Scale Rigidity

In this example we consider a rock with geomechanical behavior governed by the fine-scale Hooke's law

$$\sigma_{ij} = e\varepsilon_{ij} \quad \text{for } i = j, \qquad \sigma_{ij} = 2e_0\varepsilon_{ij} \quad \text{for } i \neq j \tag{8}$$

where $e(x, y, z) = e_0 f(x, y, z)$ with constant e_0. The heterogeneity is described by

$$f(x, y, z) = \frac{8abc \cosh^2 x \cosh^2 y \cosh^2 z}{(a + \frac{1}{2}\sinh 2a)(b + \frac{1}{2}\sinh 2b)(c + \frac{1}{2}\sin 2c)} \tag{9}$$

in the domain $-a \leq x \leq a$; $-b \leq y \leq b$; $-c \leq z \leq c$, where $a > 0, b > 0$, and $0 < c < \pi/2$. Outside this domain the function $f(x, y, z)$ is continued periodically, which means that $\Delta x = 2a$, $\Delta y = 2b$, and $\Delta z = 2c$ are the smallest periodicity intervals. The function $f(x, y, z)$ has been chosen such that $\langle f \rangle = 1$.

The following nine fine-scale displacement vectors satisfy the equilibrium equation combined with Hooke's law [Eq. (3)] and the nine orthonormal boundary conditions (5)

$$(u_{11x}, u_{11y}, u_{11z}) = (a \coth a \tanh x, 0, 0) \tag{10.1}$$

$$(u_{22x}, u_{22y}, u_{22z}) = (0, b \coth b \tanh y, 0) \tag{10.2}$$

Table 3. Exact Rigidities (kPa) Derived From Equation (7)

$C\ldots$	$xx..$	$yy..$	$zz..$	$xy..$	$yz..$	$zx..$
$..xx$	249.9792461	79.30399937	0.040642132	0	0	0
$..yy$	79.30399937	249.9792461	0.040642132	0	0	0
$..zz$	0.040642132	0.040642132	0.109754705	0	0	0
$..xy$	0	0	0	85.33762335	0	0
$..yz$	0	0	0	0	0.035351296	0
$..zx$	0	0	0	0	0	0.035351296

Table 4. Numerically Approximated Rigidities (kPa) Using Displacement–Stress Averaging

$C....$	$xx..$	$yy..$	$zz..$	$xy..$	$yz..$	$zx..$
$..xx$	2.4992E + 02	7.9304E + 01	4.0641E − 02	1.6146E − 10	2.3760E − 07	1.8819E − 07
$..yy$	7.9304E + 01	2.4992E + 02	4.0641E − 02	1.7684E − 11	5.8990E − 07	7.7998E − 08
$..zz$	4.0641E − 02	4.0641E − 02	1.0980E − 01	−1.4269E − 14	1.0665E − 11	5.4853E − 11
$..xy$	−1.0383E − 10	−8.3828E − 11	8.0218E − 11	8.5344E + 01	5.5136E − 08	1.7612E − 07
$..yz$	2.3762E − 07	5.8989E − 07	6.6321E − 11	5.5117E − 08	3.5350E − 02	−7.9291E − 12
$..zx$	−1.3443E − 11	4.9497E − 12	4.2043E − 11	−3.0327E − 11	6.2305E − 15	3.5350E − 02

Table 5. Numerically Approximated Rigidities (kPa) Using Displacement–Energy Averaging

$C_{\ldots\ldots}$	$xx_{\ldots}$	$yy_{\ldots}$	$zz_{\ldots}$	$xy_{\ldots}$	$yz_{\ldots}$	$zx_{\ldots}$
$\ldots xx$	2.4992E + 02	7.9304E + 01	4.0644E − 02	−9.0842E − 11	2.3759E − 07	−1.3357E − 11
$\ldots yy$	7.9304E + 01	2.4992E + 02	4.0644E − 02	−6.6709E − 11	5.8986E − 07	5.0597E − 12
$\ldots zz$	4.0639E − 02	4.0639E − 02	1.0980E − 01	−1.4314E − 15	1.0454E − 11	3.3181E − 11
$\ldots xy$	8.1736E − 11	9.4891E − 11	5.9265E − 14	8.5344E + 01	5.5117E − 08	−3.0326E − 11
$\ldots yz$	2.3757E − 07	5.8969E − 07	1.0524E − 11	5.5136E − 08	3.5349E − 02	2.1026E − 16
$\ldots zx$	−1.3413E − 11	5.1727E − 12	3.2871E − 11	−3.0262E − 11	−1.8423E − 15	3.5349E − 02

$$(u_{33x}, u_{33y}, u_{33z}) = (0, 0\ c\cot c\ \tan z) \tag{10.3}$$

$$u_{\alpha\beta i} = \delta_{i\beta} x_\alpha, \quad \alpha \neq \beta \tag{10.4}$$

In this example, Hooke's law and the energy equation yield 15 nonzero fine-scale stresses σ_{mnij} and energies ϕ_{ijmn} satisfying $\sigma_{mnij} = \phi_{ijmn}$. The volume averaged stress and energy components then yield the coarse-scale rigidity components resulting in Hooke's law on the coarse scale

$$\begin{pmatrix} \Sigma_{xx} \\ \Sigma_{yy} \\ \Sigma_{zz} \end{pmatrix} = e_0 \begin{pmatrix} F_x & 0 & 0 \\ 0 & F_y & 0 \\ 0 & 0 & F_z \end{pmatrix} \cdot \begin{pmatrix} E_{xx} \\ E_{yy} \\ E_{zz} \end{pmatrix} \qquad \Sigma_{ij} = 2e_0 E_{ij} \quad \text{for } i \neq j \tag{11}$$

where

$$F_x = \frac{2a^2 \coth a}{a + \frac{1}{2}\sinh 2a}, \quad F_y = \frac{2b^2 \coth b}{b + \frac{1}{2}\sinh 2b}, \quad F_z = \frac{2c^2 \cot c}{c + \frac{1}{2}\sin 2c}. \tag{12}$$

Table 6 shows the parameters used in the numerical example, while the exact coarse-scale rigidities are shown in Table 7. The numerical analyses have been performed using a $\Delta x \times \Delta y \times \Delta z$ mesh refinement sequence of $10 \times 10 \times 5$, $20 \times 20 \times 10$, and $40 \times 40 \times 20$. The rigidities are approximated as piecewise constant, in such a way that the approximate rigidity in each solid block equals the exact rigidity in the center of that block. Figure 4 visualizes the approximate rigidity distribution of the $40 \times 40 \times 20$ model. Numerical approximations for this $40 \times 40 \times 20$ mesh are presented in Tables 8 and 9 for respectively displacement–stress and displacement–energy averaging. The approximation has an accuracy of 2%, except for component C^{NB}_{zzzz}, which is a factor 2.67 too large. This large error is caused by the fine-scale rigidities are the z-boundaries, which are approximated as 12 times larger than the exact rigidities. Figure 5 shows the sum $C^{\mathrm{NB}}_{xxxx} + C^{\mathrm{NB}}_{yyyy} + C^{\mathrm{NB}}_{zzzz}$ of the numerically approximated coarse-scale rigidity tensor as it converges to the exact solution under grid refinement.

Table 6. Parameters of Example With Continuous Fine-Scale Rigidity

a	π
b	π
c	$(49/100)\pi$
e_0	100 kPa

Table 7. Exact Coarse-Scale Rigidities (kPa) Derived From Equation (12)

C....	*xx*..	*yy*..	*zz*..	*xy*..	*yz*..	*zx*..
..*xx*	1.44913E + 04	0	0	0	0	0
..*yy*	0	1.44913E + 04	0	0	0	0
..*zz*	0	0	9.48201E + 03	0	0	0
..*xy*	0	0	0	5.00000E + 04	0	0
..*yz*	0	0	0	0	5.00000E + 04	0
..*zx*	0	0	0	0	0	5.00000E + 04

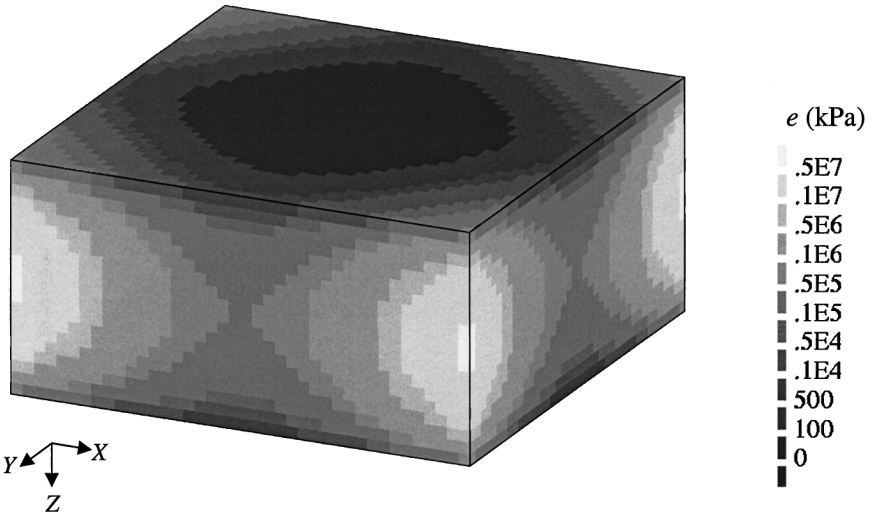

Figure 4. Piecewise constant approximation of continuous rigidity distribution.

FIELD EXAMPLE

The heterogeneity pattern of the fine-scale rigidity is taken from a field example. We consider a homogenization cell that is part an oil reservoir. Within this cell the absolute permeability $k(x, y, z)$ is known (Zijl and Trykozko, 2001). We may reasonably assume that the heterogeneity pattern of the rigidity is the same as that of the permeability. There exists no unique physical relation between permeability and rigidity. However, for the sake of providing an example, a simple but reasonable relationship will be postulated.

For isotropic media, Young's modulus and Poisson's ratio can be uniquely related to the seismic velocities v_s and v_p : $e/4\rho v_s^2 = 1 - (1 - v_s^2/v_p^2)^{-1}/4$, $\nu = 1 - (1 - v_s^2/v_p^2)^{-1}/2$ (Helbig, 1994).

Table 8. Numerically Approximated Rigidities (kPa) Using Displacement–Stress Averaging

$C....$	$xx..$	$yy..$	$zz..$	$xy..$	$yz..$	$zx..$
$..xx$	1.44E + 04	1.67E + 00	−5.27E − 03	5.38E − 03	−4.33E − 05	−3.13E − 04
$..yy$	1.67E + 00	1.44E + 04	−5.16E − 03	−4.94E − 03	−2.73E − 04	−1.97E − 05
$..zz$	−6.51E − 06	1.23E − 06	2.53E + 04	−2.08E − 06	−2.92E − 04	1.84E − 04
$..xy$	−4.11E − 04	2.64E − 03	6.95E − 05	4.88E + 04	1.85E − 04	−1.58E − 04
$..yz$	9.48E − 06	2.00E − 04	−1.75E − 03	−8.88E − 05	4.97E + 04	−5.23E − 03
$..zx$	−5.79E − 04	3.15E − 05	8.82E − 04	6.12E − 05	6.89E − 05	4.97E + 04

Table 9. Numerically Approximated Rigidities (kPa) Using Displacement–Energy Averaging

$C....$	$xx..$	$yy..$	$zz..$	$xy..$	$yz..$	$zx..$
$..xx$	1.45E + 04	−5.12E − 01	−9.51E − 04	6.32E − 03	−1.25E − 05	−2.06E − 04
$..yy$	−5.12E − 01	1.45E + 04	−1.02E − 03	−4.72E − 03	−6.79E − 05	1.50E − 05
$..zz$	−8.47E − 04	−7.92E − 04	2.53E + 04	7.25E − 05	−4.09E − 04	1.97E − 04
$..xy$	5.41E − 03	−4.05E − 03	6.27E − 05	5.00E + 04	−1.96E − 05	3.38E − 04
$..yz$	−6.48E − 05	−2.52E − 04	4.18E − 04	1.60E − 04	4.99E + 04	−6.05E − 03
$..zx$	−3.44E − 04	−2.57E − 05	1.20E − 04	−1.54E − 04	−5.07E − 03	4.99E + 04

Let us now consider rock types in which a high permeability correlates with a high porosity. For such rocks, high permeability regions may contain relatively large amouts of fluids (water, oil, gas), which have a nonzero compression modulus κ and a vanishing shear modulus $\mu \to 0$. Hence, fluids have a vanishing Young's modulus $e = 9\kappa\mu/(3\kappa + \mu) \to 0$ (Davis and Selvadurai, 1996). Therefore, for such rock types it is reasonable to assign a relatively low shear velocity v_s to high permeability regions. On the other hand, low permeability rocks that contain hardly liquids, will have a relatively high shear velocity. Making these qualitative assumptions quantitative, we assume that the shear wave velocity is given by $v_s^2 = \alpha k^{-1}$ with $\alpha = 0.25 \times 10^{-6}\,\mathrm{m}^4 \cdot \mathrm{s}^{-2} = 0.25 \times 10^{9}\mathrm{m}^2 \cdot \mathrm{s}^{-2} \cdot \mathrm{mDa}$ (De Haan, Giesen, and Scheffers, 2000).

Real rocks have material properties such that $0 < v_s^2/v_p^2 < 1/2$, hence $2\rho v_s^2 < e < 3\rho v_s^2$ and $0 < v < 1/2$. As postulated above, pieces of rock with a relatively

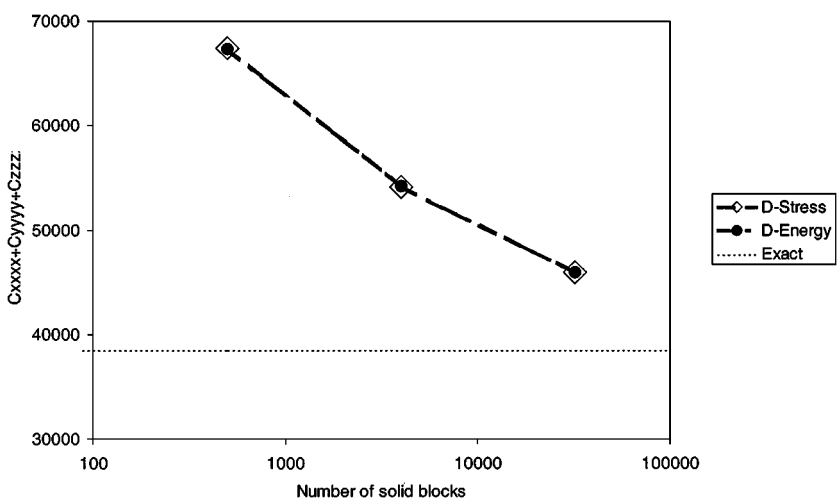

Figure 5. Sum $C^{\mathrm{NB}}_{xxxx} + C^{\mathrm{NB}}_{yyyy} + C^{\mathrm{NB}}_{zzzz}$ as a function of the number of solid blocks.

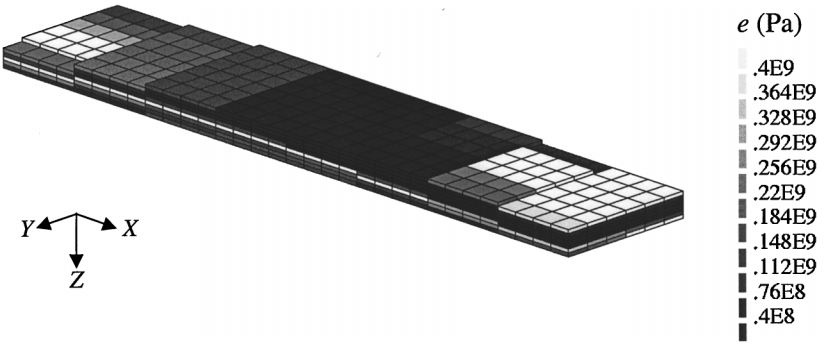

Figure 6. Fine-scale rigidity distribution of field example; inactive cells have been omitted.

low shear wave velocity (i.e., a relatively high permeability and porosity) contain relatively large amounts of fluid. Since for fluids $\mu \to 0$, Poisson's ratio $\nu = (3\kappa - 2\mu)/(6\kappa + 2\mu) \to 1/2$ (Davis and Selvadurai, 1996). In contrast, for pieces of rock with a relatively high shear velocity, Poisson's ratio is assumed to be much smaller than 1/2. This will be accomplished by choosing v_p^2 equal to two times the maximum value of v_s^2 in the homogenization cell.

Finally, since fluids ($\nu \to 1/2$) are less dense than solids ($0 \leq \nu < 1/2$) the density is chosen as $\rho = 2000(1 - \nu)$ kg $\cdot$ m^{-3}.

In this field example $k(x, y, z)$ varies from 213.188 to 13984.5 mDa. According to the above "translation rules," Young's modulus $e(x, y, z)$ varies from 54 to 4691 MPa (Fig. 6) and Poisson's ratio $\nu(x, y, z)$ varies from 0 to 0.4961. The homogenization cell consists of $6 \times 8 \times 8 = 384$ hexahedral cells, each with a given permeability. There are 26 "inactive" cells to which the small permeability $k = 1$ mDa has been assigned. In our geomechanical model these cells are extremely rigid ($e = 2004$ GPa). In Figure 6, which shows the fine-scale rigidity distribution, the inactive cells are removed. The geometry of this cell is very anisotropic; the aspect ratio $\Delta x/\Delta z$ is equal to 6, while the aspect ratio $\Delta y/\Delta z$ is equal to 25.

Figure 7 shows the different meshes used in the analyses. Table 10 shows the dimensions of the solid blocks of the different meshes. The coarse-scale rigidity components of the finite element model with 1536 elements are given in the Tables 11 and 12. Note that the displacement–stress averaging method gives an approximately symmetric matrix while the displacement–energy averaging yields an exactly symmetric matrix. In Figure 8(a)–(f) the six diagonal components of the coarse-scale rigidity matrix are plotted as a function of the mesh size. We observe that these components decrease monotonically when refining the mesh, which is in agreement with the upper bound properties of the node-based finite element method.

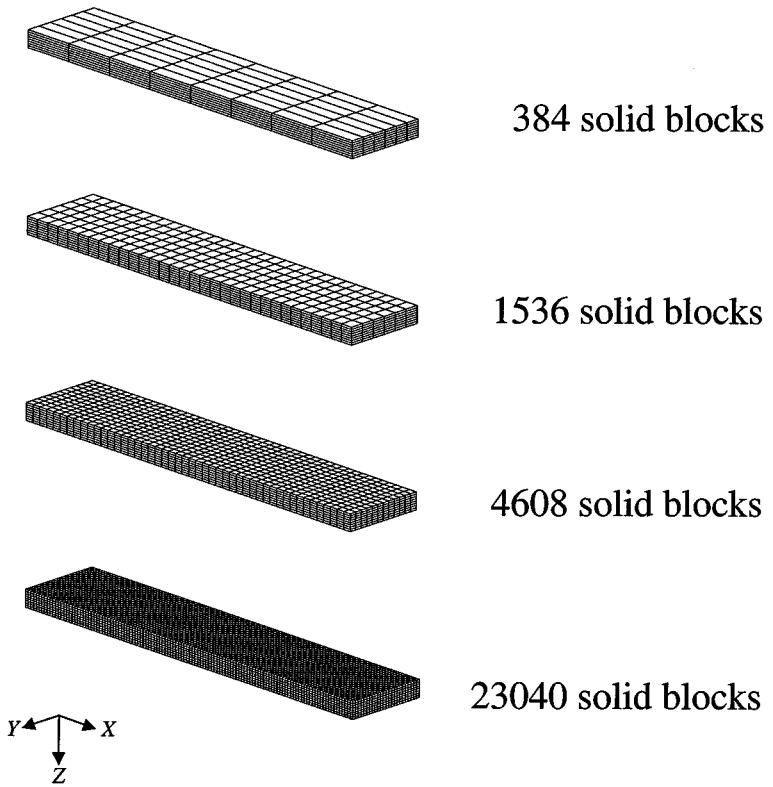

Figure 7. Sequence of refined meshes for field example.

CONCLUSIONS

The fine-scale Young's modulus and Poisson's ratio of the geological data model have been homogenized. The resulting coarse-scale rigidities relate the volume-averaged displacement, strain, stress, and energy in such a way that the equilibrium equation, Hooke's law, and the energy equation preserve the well-known form these expressions have on the fine scale.

Table 10. Dimensions of Solid Block in the Different Meshes

No. of solid blocks	Division	No. of nodes	Solid block size (m^3)
384	$6 \times 8 \times 8$	567	$6 \times 40 \times 150$
1536	$6 \times 8 \times 32$	2079	$6 \times 40 \times 37.5$
4608	$6 \times 16 \times 48$	5831	$6 \times 20 \times 25$
23040	$6 \times 32 \times 120$	27951	$6 \times 10 \times 10$

Table 11. Numerically Approximated Rigidities (kPa) Using Displacement–Stress Averaging

$C....$	$xx..$	$yy..$	$zz..$	$xy..$	$yz..$	$zx..$
$..xx$	3.533E + 06	2.223E + 06	2.303E + 06	−3.548E + 03	−1.081E + 02	6.706E + 03
$..yy$	2.230E + 06	1.313E + 08	2.249E + 06	−7.299E + 03	−3.655E + 02	3.470E + 02
$..zz$	2.302E + 06	2.242E + 06	2.682E + 06	4.279E + 02	3.665E + 01	−9.533E + 02
$..xy$	−3.429E + 03	−5.551E + 02	5.612E + 02	1.783E + 05	1.228E + 03	−3.707E + 01
$..yz$	−1.087E + 02	−2.456E + 02	3.730E + 01	1.231E + 03	3.799E + 04	−3.094E + 00
$..zx$	6.712E + 03	3.234E + 02	−9.801E + 02	−3.665E + 01	−6.894E + 00	3.640E + 04

Table 12. Numerically Approximated Rigidities (kPa) Using Displacement–Energy Averaging

$C....$	$xx..$	$yy..$	$zz..$	$xy..$	$yz..$	$zx..$
$..xx$	3.691E + 06	2.230E + 06	2.291E + 06	1.086E + 03	−1.807E + 02	8.032E + 03
$..yy$	2.230E + 06	1.332E + 08	2.241E + 06	1.849E + 02	−1.298E + 02	4.072E + 02
$..zz$	2.291E + 06	2.241E + 06	2.726E + 06	3.059E + 02	−5.489E + 01	−1.276E + 03
$..xy$	1.086E + 03	1.885E + 02	3.052E + 02	1.934E + 05	1.373E + 03	5.442E + 01
$..yz$	−1.809E + 02	−1.299E + 02	−5.520E + 01	1.373E + 03	3.957E + 04	−1.210E + 01
$..zx$	8.032E + 03	4.070E + 02	−1.277E + 03	5.439E + 01	−1.212E + 01	3.801E + 04

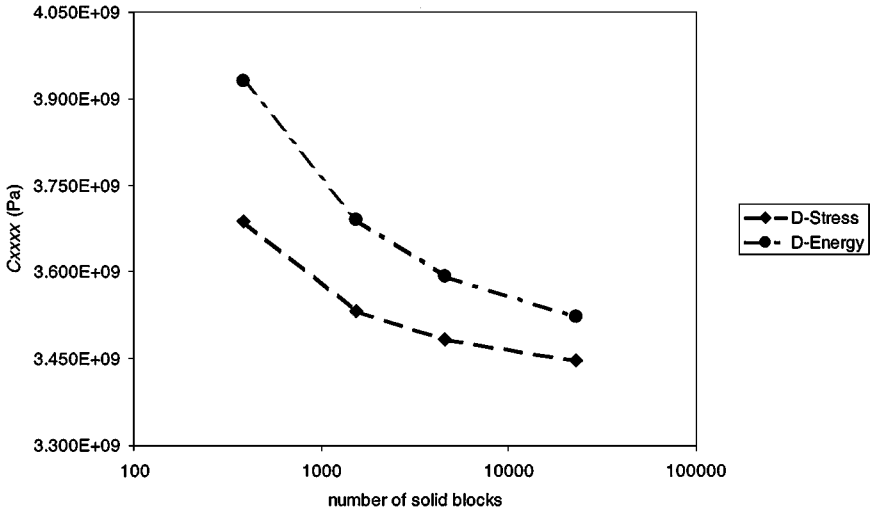

a)

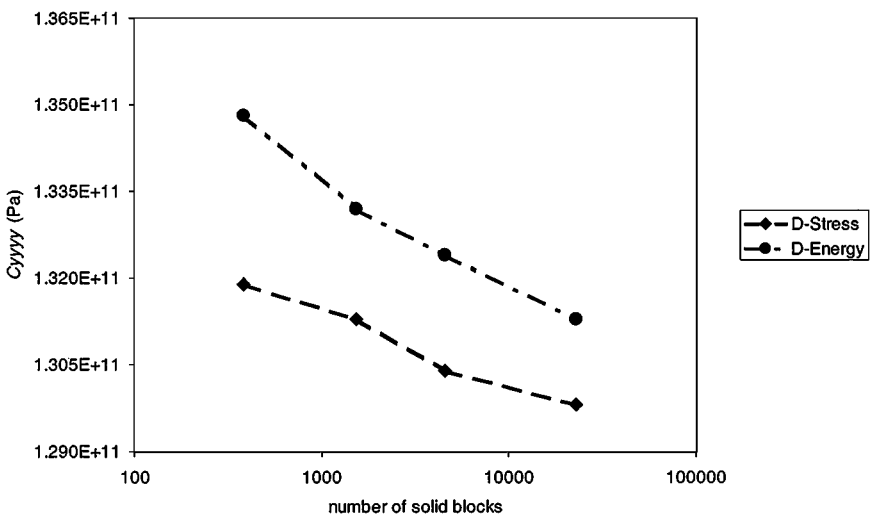

b)

Figure 8. (a) Coarse-scale rigidity C^{NB}_{xxxx} for the sequence of refined meshes; (b) coarse-scale rigidity C^{NB}_{yyyy} for the sequence of refined meshes; (c) coarse-scale rigidity C^{NB}_{zzzz} for the sequence of refined meshes; (d) coarse-scale rigidity C^{NB}_{xxyy} for the sequence of refined meshes; (e) coarse-scale rigidity C^{NB}_{yyzz} for the sequence of refined meshes; (f) coarse-scale rigidity C^{NB}_{zzxx} for the sequence of refined meshes.

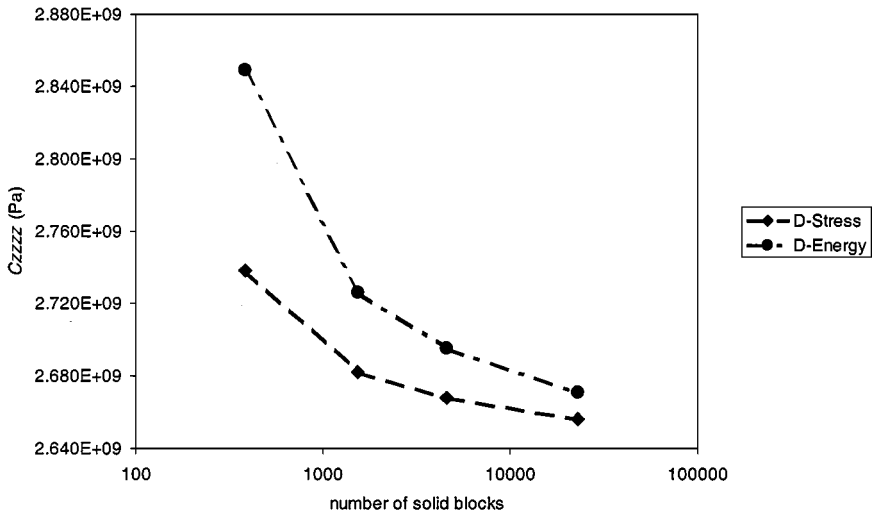

c)

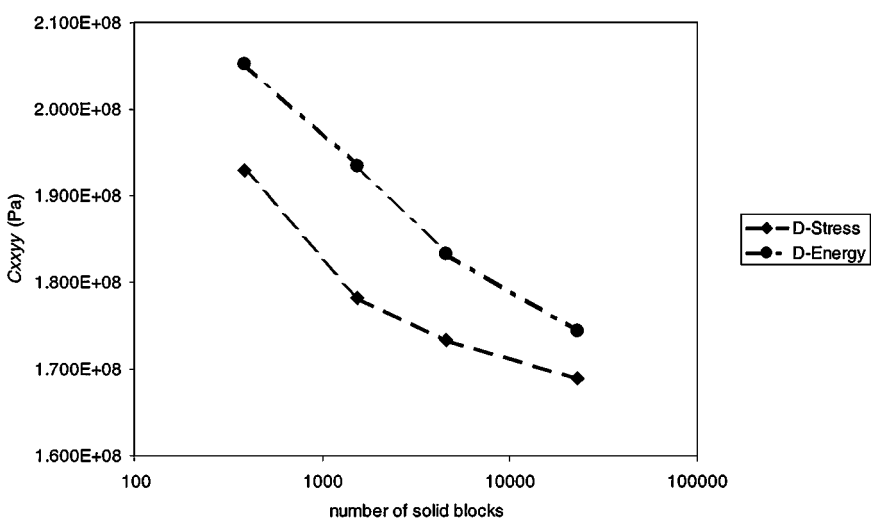

d)

Figure 8. (*Continued*)

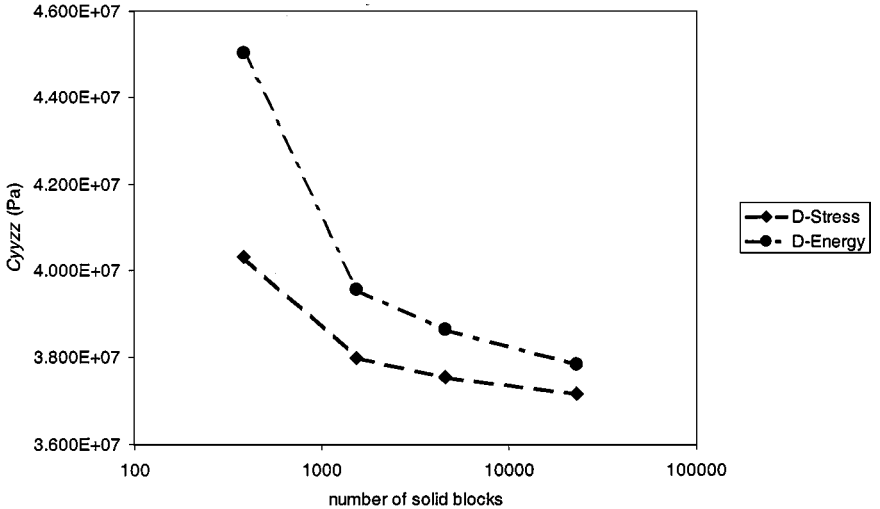

e)

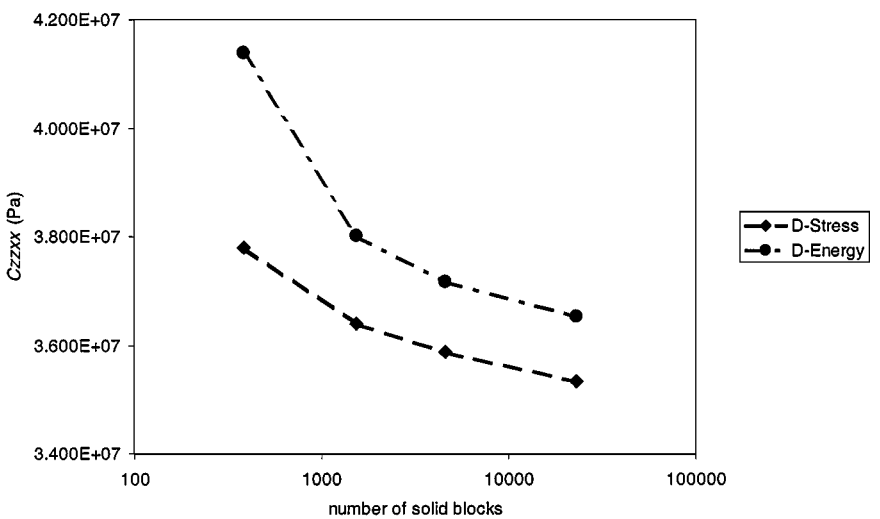

f)

Figure 8. (*Continued*)

The theory of homogenization has been presented in a simple way based on physical understanding. Two independent approaches can be distinguished: displacement–stress (DS) averaging and displacement–energy (DE) averaging. Under the simplifying assumption of spatial periodicity these two approaches yield the same coarse-scale rigidity (cf. Appendix for a proof).

The spatial distribution of the rigidity is generally so complex that exact solutions of the homogenization equations cannot be found. Therefore, numerical approximation methods have been applied. Software for the numerical homogenization of 3D spatial distributions of the rigidity has been implemented in the finite element package DIANA, which is based on the node-based finite element method for the displacement as primary variable. It is shown that this method is an upper bound method for the diagonal components of the coarse-scale rigidity matrix.

The software module has been validated extensively by a number of synthetic and field-data tests. Moreover, the numerical homogenization model has been applied to three examples to estimate the numerical error as a function of the mesh density.

REFERENCES

Arbogast, T., Wheeler, M. F., and Yotov, I., 1997, Mixed finite elements for elliptic problems with tensor coefficients as cell-centered finite differences: SIAM J. Numer. Anal., v. 34, no. 2, p. 828–852.

Auriault, J.-L., 1983, Effective macroscopic description for heat conduction in periodic composites: Int. J. Heat Mass Transfer, v. 26, no. 6, p. 861–869.

Bakhvalov, N., and Panansenko, G., 1994, Homogenization: Averaging processes in periodic media: Kluwer, Dordrecht, 354 p.

Bensoussan, A., Lions, J.-L., and Papanicolaou, G., 1978, Asymptotic analysis for periodic structures: North Holland, Amsterdam, 200 p.

Bossavit, A., 1998, Computational electromagnetism, variational formulations, complementarity, edge elements: Academic Press, San Diego, 321 p.

Davis, R. O., and Selvadurai, A. P. S., 1996, Elasticity and geomechanics: Cambridge University Press, New York, 371 p.

De Haan, H., Giesen, M., and Scheffers, B., 2000, Comparison of velocity models for 2D time-depth conversion of the Chalk Group: Inf.—TNO-NITG Ed. Geo-Energy, v. 5, May, p. 1–4.

De Witte, F. C., and Hendriks, M. A. N., 1998, Diana—finite element analysis, user's manual release 7, linear static analysis: TNO Building and Construction Research, Delft, 217 p.

Dogru, A. H., 2000, Megacell reservoir simulation: J. Pet. Technol., May, p. 54–60.

Duvaut, G., and Lions, J.-L., 1976, Inequalities in mechanics and physics: Springer, Berlin, 397 p.

Helbig, K., 1994, Foundations of aniosotropy for exploration seismics: Pergamon, New York, 486 p.

Hornung, U., 1997, Homogenization and porous media: Springer, Berlin, 381 p.

Lanczos, C., 1970, The variational principles of mechanics: Dover, New York, 319 p.

Lefik, M., and Schrefler, B. A., 1994, Application of the homogenisation method to the analysis of superconducting coils: Fusion Eng. Des., v. 24, p. 231–255.

Morse, Ph. M., and Feshbach, H., 1953, Methods of theoretical Physics: McGraw-Hill, New York, 1978 p.

Pellegrino, C., Galvanetto, U., and Schrefler, B. A., 1999, Numerical homogenization of periodic composite materials with non-linear material components: Int. J. Numer. Methods Eng., v. 46, p. 1609–1637.

Penman, J., 1988, Dual and complementary variational techniques for the calculation of electromagnetic fields: Adv. Electron. Electron Phys., v. 70, p. 315–364.

Rijpsma, G., and Zijl, W., 1998, Upscaling of Hooke's law for imperfectly layered rocks: Math. Geol., v. 30, no. 8, p. 943–969.

Sanchez-Palencia, E., 1980, Non-homogeneous media and vibration theory, *in* Lecture notes in Physics, Vol. 127: Springer, Berlin, 415 p.

Schrefler, B. A., Lefik, M., and Galvanetto, U., 1997, Correctors in a beam model for unidirectional composites: Mech. Computational Mater. Struct., v. 4, p. 159–190.

Strang, G., and Fix, G. J., 1973, An analysis of the finite element method: Prentice-Hall, Englewood Cliffs, NJ, 306 p.

Trykozko, A., Zijl, W., and Bossavit, A., 2001, Nodal and mixed finite elements for the numerical homogenization of 3D permeability: Computational Geosciences, v. 5, p. 61–84.

Van Dyke, M., 1975, Perturbation methods in fluid mechanics: Parabolic Press, Stanford, 271 p.

Zijl, W., and Trykozko, A., 2001-a, Numerical homogenization of the absolute permeability using the conformal-nodal and mixed-hybrid finite element method: Transp. Porous Media., v. 44, p. 33–52.

Zijl, W., and Trykozko, A., 2001-b, Numerical homogenization of the absolute permeability tensor around a well: SPE J., p. 399–408.

APPENDIX: EQUIVALENCE OF DISPLACEMENT–STRESS AND DISPLACEMENT–ENERGY AVERAGING

Displacement and Strain

Homogenization is a method of upscaling in which constant displacement differences between equivalent points on two opposite boundaries of the homogenization cell are specified as boundary conditions. As a consequence, the volume-averaged displacement is a linear function of the Cartesian coordinates

$$U_i(\underline{x}) = \langle u_i \rangle(\underline{x}) = U_i^{(0)} + A_{ij} x_j \tag{A1}$$

where $U_i^{(0)}$ and A_{ij} are constants. In case of orthonormal boundary conditions, the nine constants are $A_{ij} = \delta_{in}\delta_{jm}$, where each pair $m, n = 1, 2, 3$ represents a particular choice—a load case—with nine coarse-scale displacements U_{mni}, $i = 1, 2, 3$. Although orthonormal boundary conditions greatly simplify actual computations, they are not required in the following proof; *constant* displacement differences suffice. Then, the fine-scale displacements can be written as a vector that is linear in the spatial coordinates plus a periodic vector function. (A periodic function has *zero* differences between equivalent points on two opposite boundaries of the homogenization cell.)

$$u_i(\underline{x}) = U_i^{(0)} + A_{ij} x_j + \chi_i(\underline{x}), \tag{A2}$$

Taking the symmetric part of the gradient yields

$$\varepsilon_{ij}(x) = \frac{1}{2}(\partial_i u_j(\underline{x}) + \partial_j u_i(\underline{x})) = E_{ij} + \frac{1}{2}(\partial_i \chi_j(\underline{x}) + \partial_j \chi_i(\underline{x})) \tag{A3}$$

where $E_{ij} = (A_{ij} + A_{ji})/2$. Integration over the periodic homogenization cell Ω with volume $V = \iiint_\Omega dV$ yields

$$\iiint_\Omega \varepsilon_{ij}(x)\, dV = E_{ij} V + \iiint_\Omega \frac{1}{2}(\partial_i \chi_j(\underline{x}) + \partial_j \chi_i(\underline{x}))dV. \tag{A4}$$

Since $\chi_i(x)$ is a periodic vector function, the volume average of its gradient is equal to 0. Hence

$$E_{ij} = \frac{1}{V} \iiint_\Omega \varepsilon_{ij}(\underline{x})\, dV = \langle \varepsilon_{ij} \rangle \tag{A5}$$

which proves that the coarse-scale strain E_{ij} is equal to the volume average of the fine-scale strain $\langle \varepsilon_{ij} \rangle$.

The Basic Approach to Homogenization

From the physical point of view expounded in this paper, homogenization is based on the following requirement [Eq. (2)]

$$\partial_i \sigma_{ij}(\underline{x}) = \partial_i \Sigma_{ij}(\underline{x}), \tag{A6}$$

Below, Equation (A6) will be applied in two different ways.

First Application of Basic Requirement

For periodic media, the coarse-scale stress is constant. Substitution of constant Σ_{ij} into the right-hand side of Equation (A6) yields

$$\partial_i \sigma_{ij}(\underline{x}) = \partial_i (c_{ijmn}(\underline{x})[\partial u]_{mn}(\underline{x})) = 0 \tag{A7}$$

where the shorthand notation $[\partial u]_{ij} = (\partial_i u_j + \partial_j u_i)/2$ has been used. Equation (A7) has to be solved in at least one periodicity cell with periodic boundary conditions for the vector function $\chi_i(\underline{x})$.

Second Application of Basic Requirement

Multiplying the left and right sides of Equation (A6) by an arbitrary displacement vector $v_i(x)$, applying some vector differentiation rules, and using Gauss's divergence theorem yields

$$\iiint_{\Omega} [\partial v]_{ij}(\underline{x}) C_{ijmn} [\partial U]_{mn}(\underline{x})\, dV - \iiint_{\Omega} [\partial v]_{ij}(x) c_{ijmn}(x) [\partial u]_{mn}(x)\, dV$$
$$= -\oiint_{\partial\Omega} v_i(x)\{\sigma_{ij}(x) - \Sigma_{ij}\} n_j\, dS \tag{A8}$$

where the circle in the surface integrals means integration over the closed boundary $\partial\Omega$ of the periodicity cell Ω (i.e., the homogenization cell). Let us consider in more detail the surface integral

$$\Im = \oiint_{\partial\Omega} v_i(x)\{\sigma_{ij}(\underline{x}) - \Sigma_{ij}\} n_j\, dS \tag{A9}$$

Similar to Equation (A1), the displacement vector $v_i(\underline{x})$ is written as $v_i(\underline{x}) = V_i^{(0)} + B_{ij}x_j + \kappa_i(\underline{x})$, where $V_i^{(0)}$ is a constant vector, B_{ij} is a constant tensor, and $\kappa_i(\underline{x})$ is a periodic vector function. Hence,

$$\Im = \oiint_{\partial\Omega} \left(V_i^{(0)} + \kappa_i(\underline{x}) + B_{ij}x_j\right)(\sigma_{ij}(\underline{x}) - \Sigma_{ij}) n_j\, dS$$
$$= \Im^{(1)} + \Im^{(2)} + \Im^{(3)} \tag{A10}$$

Using Equation (A6) we find

$$\Im^{(1)} = V_i^{(0)} \oiint_{\partial\Omega} (\sigma_{ij}(\underline{x}) - \Sigma_{ij}) n_j\, dS$$
$$= V_i^{(0)} \iiint_{\Omega} \partial_i (\sigma_{ij}(\underline{x}) - \Sigma_{ij})\, dV = 0 \tag{A11}$$

Using the periodic boundary conditions of $\kappa_i(\underline{x})$ and the periodicity of $\sigma_{ij}(\underline{x})$ we find

$$\Im^{(2)} = \oiint_{\partial\Omega} \kappa_i(\underline{x})(\sigma_{ij}(\underline{x}) - \Sigma_{ij}) n_j\, dS = 0 \tag{A12}$$

The evaluation of $\Im^{(3)}$ is more complex, but also more rewarding. Again using Equation (A6) we find

$$\Im^{(3)} = \oiint_{\partial\Omega} (B_{ij}x_j)(\sigma_{ij}(\underline{x}) - \Sigma_{ij}) n_j\, dS$$
$$= -B_{ij} \left(\Sigma_{ij} V - \iiint_{\Omega} \sigma_{ij}(\underline{x})\, dV \right) \tag{A13}$$

Requiring $\Im^{(3)} = 0$, which is equivalent with displacement–energy averaging (see ahead), a similar expression as Equation (A5) is found

$$\Sigma_{ij} = \frac{1}{V} \iiint_{\Omega} \sigma_{ij}(\underline{x})\, dV = \langle \sigma_{ij} \rangle \tag{A14}$$

which proves that the coarse-scale stress is equal to the volume average of the fine-scale stress.

From Equations (A11) and (A12) it follows that requiring $\Im^{(3)} = 0$ yields $\Im = 0$, that is, then the surface integral in Equation (A8) is required to be equal to 0

$$\left(\iiint_{\Omega} [\partial v]_{ij}(\underline{x})\, dV \right) C_{ijmn} [\partial U]_{mn} = \iiint_{\Omega} [\partial v]_{ij}(\underline{x}) c_{ijmn}(\underline{x}) [\partial u]_{mn}(\underline{x})\, dV \tag{A15}$$

Defining $\varepsilon_{\alpha\beta ij} = [\partial v]_{ij}$, $\varepsilon_{\gamma\delta ij} = [\partial u]_{ij}$ and using Equation (A5) shows that Equation (A15) is equivalent with the displacement–energy definition of the coarse-scale rigidity C_{ijmn}

$$\langle \varepsilon_{\alpha\beta ij} \rangle C_{ijmn} \langle \varepsilon_{\gamma\delta mn} \rangle = \langle \varepsilon_{\alpha\beta ij} c_{ijmn} \varepsilon_{\gamma\delta ij} \rangle \tag{A16}$$

In conclusion, for periodic media displacement–energy averaging (i.e., requiring Equation (A16) be satisfied) implies displacement–stress averaging (i.e., Equation (A14) holds). Moreover, it can easily be observed from Equation (A13) that the inverse is also true: displacement–stress averaging implies displacement–energy averaging. This proves Equation (4).